RESEARCH PAPER

PCCP
www.rsc.org/pccp

The role of surface electrification on the growth and structural features of titania nanoparticles

Tzvetanka Boiadjieva,† Giuseppe Cappelletti, Silvia Ardizzone,* Sandra Rondinini and Alberto Vertova

Department of Physical Chemistry and Electrochemistry, University of Milan, Via Golgi 19, 20133, Milan, Italy

Received 16th February 2004, Accepted 26th March 2004
First published as an Advance Article on the web 3rd May 2004

TiO_2 particles, prepared by following a sol–gel preparative route, were submitted to hydrothermal steps performed at solution pH values corresponding, respectively, to positive, zero and negative oxide surface charges. After the hydrothermal step all the samples were thermally treated at 300 and 600 °C, for the same length of time (6 h). The powders, both precursors and calcined samples, were characterized for phase composition–crystallinity, particle morphology and surface electrification features. The role played by the particles electrification during the hydrothermal step in affecting the physico-chemical properties of the powders is discussed.

Introduction

The understanding of the mechanisms underlying the growth of titanium dioxide polymorphs bears relevance to a very large variety of applications (paints, solar cells, gas sensors, photocatalysis, *etc.*,) with enormous economical consequences.[1–10] Of the three main TiO_2 polymorphs—anatase, rutile and brookite—the anatase form shows the highest activity for gas sensors and photocatalysis and has become a major component in electrochemical and photoelectrochemical devices.[5–8] Several properties of the oxide must be controlled, in the selected preparation route, depending on the final application. In the case of photoelectrochemical devices, nanosized anatase particles are desired to provide very large surface area and enhanced activity due to quantum confinement effects in the semiconductor space charge.[5,8,10] On the other side, a high degree of crystallinity is required at the same time; in fact, improved crystallinity removes potential trap states due to lattice imperfections in the titania nanocrystallites and thus improves conduction through the nanoporous titania network.[4] The adoption of high temperature (and/or pressure) stages in the preparation to promote crystallinity is generally not successful, as together with the possible promotion of other oxide polymorphs, mainly rutile, these treatments invariably provoke particle sintering, pore collapse, and a dramatic loss in surface area.[1]

Hydrothermal treatment represents an alternative to high temperature calcinations to promote crystallisation under milder conditions. Results are present in the literature, relative to hydrothermal preparations aimed at obtaining either titania nanoparticles or TiO_2 thin films; treatments are generally performed in the temperature range 80–240 °C.[7,9,10] Innovative is the approach by Wilson *et al.*[4] who introduce a microwave hydrothermal process to allow for rapid heating and faster processing time.

Penn *et al.*[11] have investigated the morphology development and crystal growth of titania under hydrothermal conditions. They have evidenced the occurrence of two primary coarsening mechanisms, the first leading to particle growth *via* solution, and the second which occurs by addition of solid particles to surfaces.

Following the above reported considerations, the present work was aimed at investigating the role played by electrostatic interactions taking place between the hydrous TiO_2 particles during a short hydrothermal step. As the surface electrification of an oxide depends on the solution pH, three different conditions were selected to correspond, respectively, to positive, zero and negative oxide surface charges. The features of the aged precursor were investigated with respect to the particle morphology, surface electrification and bulk composition. The structural features of the precursor calcined at 300 and 600 °C were analyzed in detail.

Experimental

All the chemicals were of reagent grade purity and were used without further purification; doubly distilled water passed through a Milli-Q apparatus was used to prepare solutions and suspensions.

Sample preparation

The preparation of TiO_2 particles, by the sol–gel technique, was performed at room temperature as follows: a solution of 0.2 mol of $Ti(OC_3H_7)_4$ in 50 ml propanol was stirred for 30 min at 300 rpm. Then 175 ml of 0.1 M KCl, pH 3 (adjusted with diluted HCl) were added, drop by drop, fast. The slurry was kept stirred for 90 min in order to complete the hydrolysis. Subsequently, the reacting mixture was kept in the thermostated bath at 25 °C for 20 h to age.

The dried xerogel powders were purified by centrifugation–resuspension cycles and then powder fractions were aged at 80 °C at the given pH for 6 h in water. The pH of aging solutions was adjusted with diluted HCl and KOH solutions. After the aging, the suspensions were filtered and dried again at 80 °C. No washing was performed after the aging due to the low ionic strength of the aging solutions.

The samples are labeled as: TO standing for titanium dioxide, a for aged, A acid pH (pH = 3), N neutral pH (pH = 6), B basic pH (pH = 8). For example TOaN is a precursor aged at neutral pH.

† Present address: Institute of Physical Chemistry, Bulgarian Academy of Sciences, Acad. G. Bonchev, bl. 11, 1113 Sofia, Bulgaria.

DOI: 10.1039/b402370f

Finally the powders were thermally treated at 300 and 600 °C for 6 h under an oxygen stream.

Sample characterisation

Structural characterisation of the powders was performed by X-ray diffraction, using a Siemens D500 diffractometer, using Cu Kα radiation in the 10–80° 2θ angle range. The fitting program of the peaks was a particular Rietveld program,[12,13] named QUANTO,[14] devoted to the automatic estimation of the weight fraction of each crystalline phase in a mixture. The program had been also designed to estimate the amorphous content by means of the internal standard method. The internal powder, pure KCl (calcined at 200 °C), which has the same mass absorption coefficient μ (125.4 $cm^2\ g^{-1}$) of titanium dioxide (129.3 $cm^2\ g^{-1}$), was added in a known quantity (10 wt.%) to the original mixture by using a microbalance and weighing the reference and the sample directly in the X-ray sample holder.

The peak shape was fitted using a modified Pearson VII function. The background of each profile was modelled using a six-parameter polynomial in $2\theta^m$, where m is a value from 0 to 5 with six refined coefficients. When the mixture contains a certain percentage of amorphous substance, the Chebyshev function is used.

The mean dimension, d, of crystallites was obtained by elaborating the most intense X-ray peak of each phase by the Scherrer's equation,

$$d = \frac{K\lambda}{\beta \cos\theta}$$

where K is a constant related to the crystallite shape (0.9), β is the pure breadth of the powder reflection, free of the broadening due to the instrumental contributions. This calibration was performed by means of the spectrum of a standard Si powder. The accuracy with which the Scherrer's equation can be applied is limited by the uncertainties in K and by the success with which β can be deduced from the experimentally observed breadth. This equation is quite satisfactory for studies comparing the crystallite sizes of a number of samples belonging to a related series.

The method yields exhaustive values of the relative sizes even though the inflexible premises upon which the formula rests results in considerable uncertainty as to the absolute sizes.

Specific surface areas were determined by the classical BET procedure using a Coulter SA 3100 apparatus. Particle morphology was examined by scanning electron microscopy using a Cambridge 150 Stereoscan.

The distribution of ζ (zeta) Potential of particles in liquid suspension was evaluated by using a Doppler Electrophoretic Light Scattering Analyzer (DELSA 440).

Results and discussion

Fig. 1 reports the dependence of the zeta potential of the three precursor powders on the solution pH. The sample aged at neutral pH shows a regular trend, the zero zeta potential occurring at pH 5.9. This value, which represents the isoelectric point (i.e.p.) of the particles, is in full agreement with the literature data for both i.e.p. and p.z.c. (point of zero charge) for hydrous titanium dioxide particles.[15] The curve relative to the sample aged at alkaline pH is almost superimposable to the one of sample TOaN and shows that, apparently, no appreciable surface modifications have occurred during the growth at alkaline pH. The curve of the sample aged at acid pH, instead, is shifted by about one pH unit in the alkaline direction with respect to the other two curves. A shift of the isoelectric point to the alkaline direction, with respect to the pristine value, is interpreted in the literature as the result of the specific adsorption of cationic species in the inner double layer region.[16] Strong evidence is present in the literature for the occurrence of cationic soluble titanium complexes in acid solutions, mainly in the form of $Ti(OH)_2^{2+}$ which further hydrolyzes to $Ti(OH)_3^{+}$ and $Ti(OH)_4$ for increasing pH (see inset to Fig. 1).[17,18] Above pH 4, the dominance of the neutral soluble species $Ti(OH)_4$ is reported.[18] During the hydrothermal step dissolution–reprecipitation mechanisms can be expected to take place with Ostwald ripening processes leading to a decrease in the sample surface area (compare $S_{xer} = 270\ m^2\ g^{-1}$ for the un-aged precursor with the average of 220 $m^2\ g^{-1}$ of the present samples, see data in Table 1). In the case of the neutral and alkaline pH, the dissolution and re-adsorption of the neutral complexes do not modify the electrification features of the particles. In the case of the acid solution, the soluble complexes bearing a positive charge are strongly chemisorbed at the surface of the particles and provoke the observed shift of the isoelectric point.

SEM micrographs (Fig. 2) also show different features for the precursors aged at different pH values. The acid sample (Fig. 2a) shows the presence of small spheroidal particles grouped in raspberry-like aggregates; in the case of the neutral sample, instead, (Fig. 2b) the occurrence of some crystallographic organization (edge, corners, *etc.*) can be appreciated and aggregates of variable sizes (from 100 to 300 nm) can be observed. The morphology of the alkaline sample (Fig. 2c)

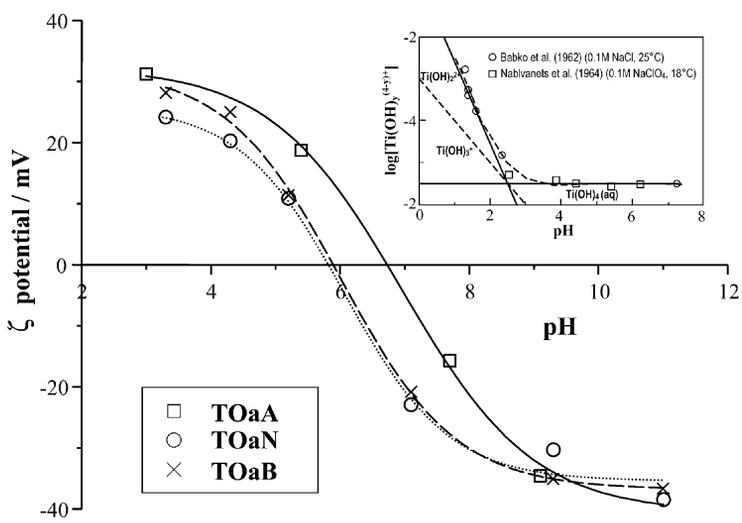

Fig. 1 Zeta potential (ζ) of the three precursor powders (TOaA, TOaN and TOaB) as a function of pH. Inset: cationic soluble titanium complexes as a function of pH solutions; redrawn from refs. 17 and 18.

Table 1 Precursor surface area and total pore volumes

Sample	$S_{B.E.T.}/m^2\ g^{-1}$	$V_{TOT}/ml\ g^{-1}$
TO	271	0.080
TOaA	215	0.332
TOaN	222	0.320
TOaB	220	0.374

does not seem to be very different from the neutral one with the sole exception of the presence of some isolated very small particles (smaller than 50 nm).

Specific surface area values are reported in Table 1 The different conditions of the hydrothermal growth do not seem to provoke relevant modifications in the extension of the interfacial contact while the introduction of the hydrothermal step provokes a definite decrease in surface area with respect to the un-aged precursor (sample named TO in the table). The comparison between the pore volume distribution of the aged samples and of the un-aged xerogel is striking (Fig. 3a). The total pore volume of the xerogel is 5–6 times lower than the one of the aged samples. The larger surface area of the xerogel is, therefore, to be mainly attributed to the occurrence of smaller particles with respect to the aged samples. Slight differences can be appreciated between the pore volumes of the aged samples. The sample aged at the i.e.p. shows the lowest total pore volume and the shape of the hysteresis loops suggests the occurrence of pores with an average bottle-neck shape (Fig. 3b). In the case of samples bearing a net surface charge, the pore volume is larger, more so in the case of the alkaline sample, especially in the region of intermediate and large pores. The shape of the hysteresis loops suggest the occurrence of open-ended tubular pores (Fig. 3b). Therefore, in the case of both acid and alkaline samples, the pores can be considered to be interparticle channels. The alkaline sample shows the occurrence of a lower degree of packing with respect to the other samples.

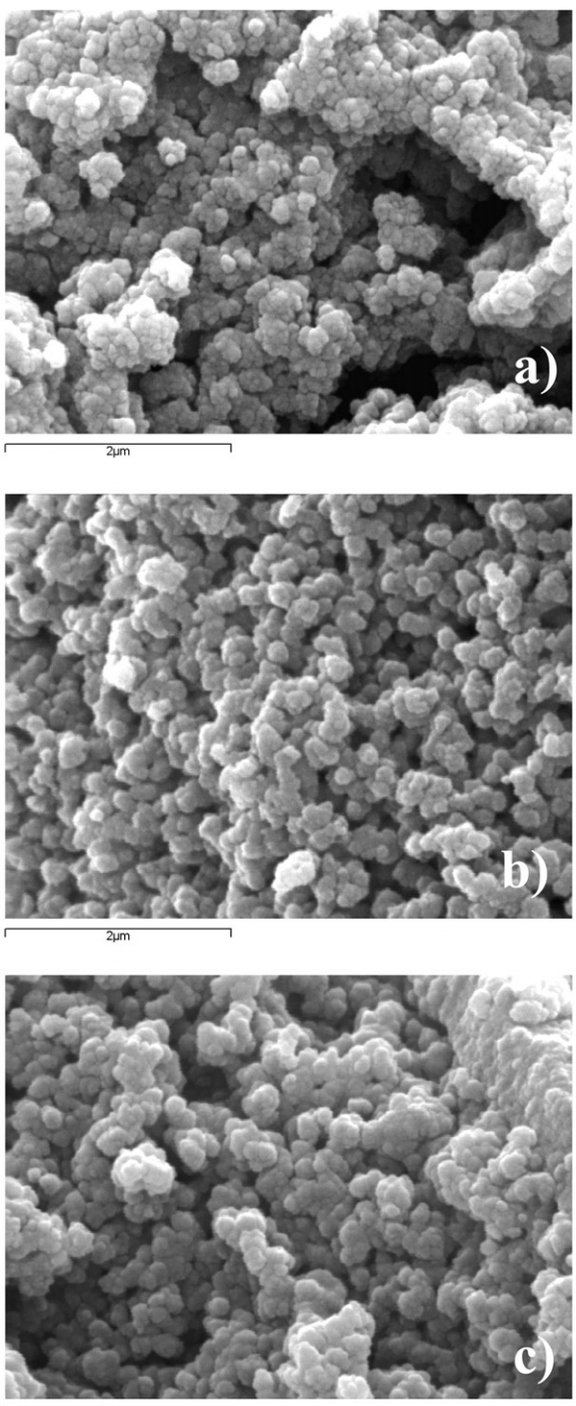

Fig. 2 SEM images of samples (a) TOaA, (b) TOaN, (c) TOaB.

To understand the effects of the hydrothermal step on the formation of the titania phases, it is important to follow the evolution of the amorphous and crystalline phases as a function of the conditions of ageing. In the specific case of the precursors (not submitted to calcination treatments) an appreciable presence of an amorphous phase can be expected and also the shape of X-ray diffraction spectra suggests that the degree of crystallinity is not high. In order to quantify the relative amounts of the different components, a modified version of the Rietveld method has been used, that allows the separation and the quantification of amorphous and crystalline phases.

Table 2 reports the phase composition of the three precursors submitted to the hydrothermal step at the three pH values. All three samples show the presence of an appreciable amorphous amount, more so for the sample aged at alkaline pH. The anatase percentage is almost invariant and the basic sample shows the lowest content of the brookite polymorph. The formation of brookite, as a minor component, during hydrothermal ageing treatments of titanium oxide hydrous precursors, is reported in the literature.[10]

Considering collectively the results from different characterizations of the precursors, some considerations can be made: (i) At acid pH the conditions of solubility are such as to provoke the formation of rounded primary particles which grow through enhanced dissolution and re-adsorption/re-precipitation mechanisms. The presence of a net positive surface charge leads to the formation of loose aggregates. (ii) At neutral pH, dissolution/re-precipitation mechanisms occur to a lesser extent and more slowly allowing the particles to develop a more ordered tridimensional organization, *i.e.* a larger fraction of crystalline material. Due to the absence of electrostatic repulsion between the particles, aggregates appear to be more packed. (iii) At alkaline pH, the conditions of solubility can be considered to be comparable to the ones of the neutral sample. The presence of the negative surface charge apparently hinders the Ostwald ripening process leading to the largest amorphous fraction. The repulsive interactions between the particles provoke a larger extent of open ended cylindrical pores in the aggregates.

For calcinations at 300 °C an appreciable amount of amorphous phase is still present and no traces of rutile are appreciable, in any case. The calcination at 300 °C does not seem to provoke relevant modifications with respect to the ageing treatment.

Important modifications occur, instead, upon calcination at 600 °C. Fig. 4 reports the phase composition and the crystallite sizes calculated by elaboration of the more intense peak with the Scherrer equation as a function of the pH conditions

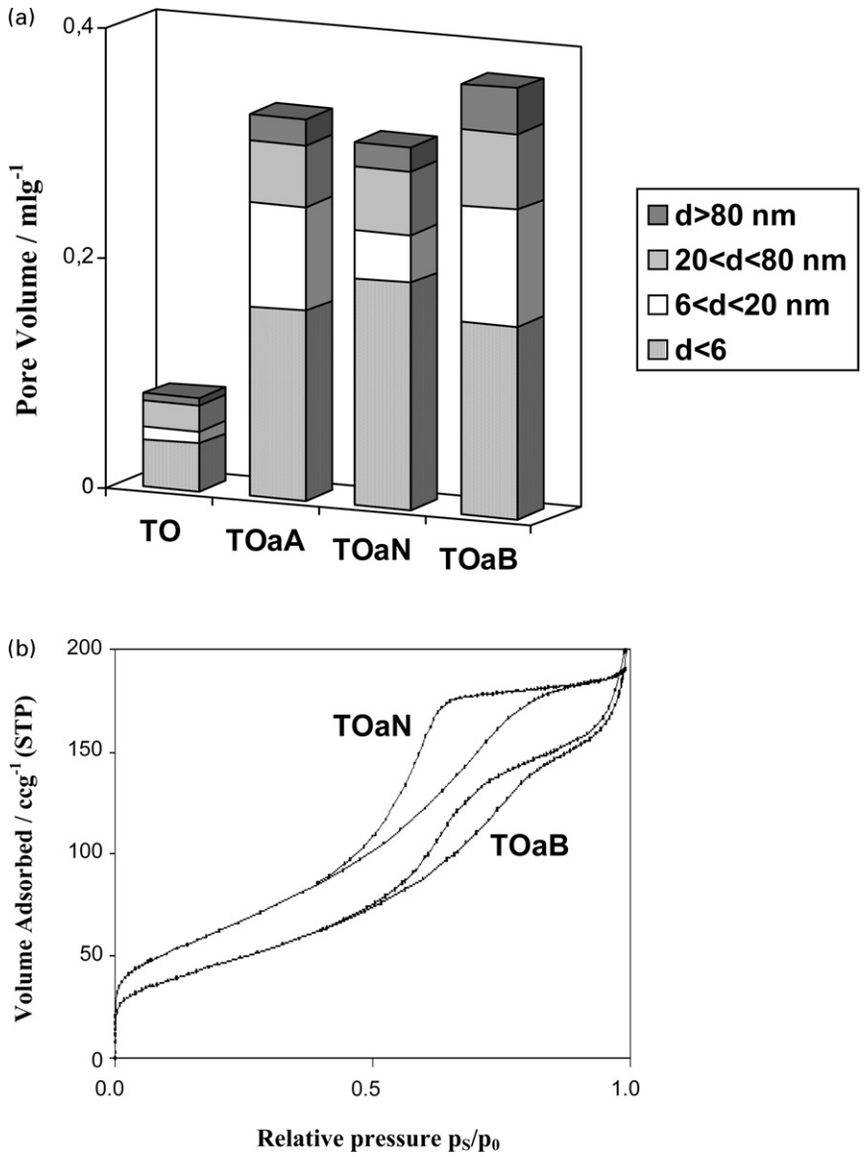

Fig. 3 (a) Distribution of pore volume of the aged samples at different pH (TOaA, TOaN and TOaB) and of the un-aged Xerogel (TO); (b) B.E.T. isotherms of TOaN and TOaB samples.

adopted during the hydrothermal growth. A difference is immediately apparent between the samples aged at the isoelectric point (pH 5.8), *i.e.* in the absence of electrostatic repulsion between the particles and the samples aged at the two pH extremes. The absence of repulsion between the particles during the hydrothermal step, supports the formation of rutile (with the consequent depression of the amount of anatase) and yields the largest crystallite sizes. In the presence of a net surface charge (either positive or negative, *i.e.* acid or neutral pH) the formation of rutile is depressed, more so in the case of the alkaline sample where the amount of rutile is lower than 4%. The sizes of the crystallites are *ca.* $\frac{1}{3}$ of the relative values at the i.e.p.

Table 2 Quantitative phase composition (A = anatase, B = brookite and amorphous) of samples hydrothermally grown at different pH and relative crystallite sizes of anatase calculated from X-ray diffractograms.

Sample	wt.% A	wt.% B	wt.% Amorphous	d_A/nm
TOaA	59.2	31.5	9.3	6.5
TOaN	60.5	31.5	7.9	6.2
TOaB	60.3	24.1	15.6	6.0

During the hydrothermal step two major coarsening mechanisms can be expected to take place.[11] The first involves single particle growth *via* addition of Ti soluble species to surfaces from solution. The second mechanism involves growth by addition of solid particles to surfaces. This latter process may occur in a precise, crystallographically controlled manner resulting in coherent interfaces. The present conditions of ageing can be considered to involve both outlined mechanisms. The different pH of growth modifies the features of the precursors, as described above, through the first, *via* solution mechanism. The different conditions of electrostatic interactions, instead, have provoked different packing factors.

Particle arrangement and packing is reported to influence the thermal stability and phase transformation of materials. Banfield *et al.*[19,20] reported that the anatase–rutile transformation could be initiated from the rutile-like elements created at the oriented contacts between anatase particles. The lack of proper particle attachment or particle coordination would, instead, decrease the possibility of rutile nucleation. The looser packing of particles generated in the hydrothermal treatment, at either positive or negative particle surface charges, might be one of the main factors responsible for the higher thermal stability of the anatase structure.

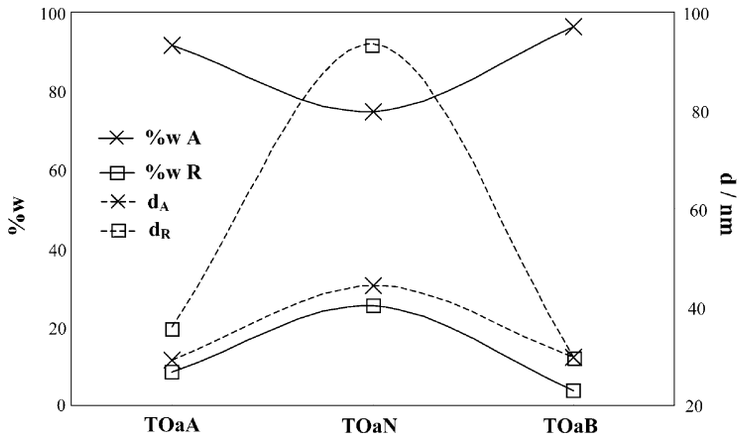

Fig. 4 Quantitative phase composition by the QUANTO elaboration of X-ray diffractograms and relative crystallite sizes by Scherrer's equation of aged samples calcined at 600 °C. Continuous curves, phase composition; dotted curves, crystallite sizes.

The phase transformation to rutile was initiated after the anatase grains have grown to a certain threshold size, *i.e. ca.* 30 nm. In literature studies[21,22] the limiting sizes reported for the formation of rutile are between 13–50 nm. The resulting rutile grains are always found to be larger than the anatase grains. In the study by Wang *et al.*[10] the critical nuclei size for rutile formation was estimated to be in the range of 40–50 nm. The authors report that once the critical size has been attained rapid rutile formation and grain growth were observed, so that the resulting rutile grains were larger than the coexisting anatase grains. This is actually the situation taking place in the present case; for particles grown at the i.e.p. the crystallite size of rutile is about 90 nm while that of anatase is about 40 nm. The critical nuclei size for phase transformation is governed by the volume free energy, surface energy and strain energy, which would vary with different materials synthesis and processing.

Conclusions

TiO_2 hydrous precursors, prepared by following a sol–gel preparative route, were submitted to hydrothermal steps at solution pH values corresponding, respectively, to positive, zero and negative oxide surface charges. During the hydrothermal step, particle growth occurs *via* dissolution/re-precipitation mechanisms which are enhanced at acid pH. The analysis of the phase composition of the aged precursors shows that anatase is the main component for all the samples together with the brookite polymorph and variable amounts of amorphous phase. The morphology of the particles shows that the samples aged in the absence of a net surface charge are composed by more packed aggregates of smaller particles.

The degree of packing of the aggregates plays a key role in imposing the anatase/rutile transformation when the samples are submitted to a thermal treatment at 600 °C. The absence of repulsion between the particles, during the hydrothermal step, supports the formation of rutile and yields the largest crystallite sizes; in the presence of a net surface charge, either positive or negative, the formation of rutile is depressed and the size of the crystallites is about one third of the relative values pertaining to the samples aged at the isoelectric point. The phase transformation to rutile is initiated after the anatase grains have grown to a threshold size of *ca.* 30 nm.

Acknowledgements

This research has been supported by a Marie Curie Fellowship of the European Community programme IMPROVING HUMAN RESEARCH POTENTIAL AND THE SOCIO-ECONOMIC KNOWLEDGE BASE-IHP under contract number HPMT-CT-2001-00314.

References

1 T. Boiadjieva, G. Cappelletti, S. Ardizzone, S. Rondinini and A. Vertova, *Phys. Chem. Chem. Phys.*, 2003, **5**, 1689.
2 A. Matsuda, Y. Kotani, T. Kogure, M. Tatsumisago and T. Minami, *J. Am. Ceram. Soc.*, 2000, **83**, 229.
3 E. Traversa, M. L. Di Vona, S. Licoccia, M. Sacerdoti, M. C. Carotta, L. Crema and G. Martinelli, *J. Sol-Gel Sci. Technol.*, 2001, **22**, 167.
4 G. J. Wilson, G. D. Will, R. L. Frost and S. A. Montgomery, *J. Mater. Chem.*, 2002, **12**, 1787.
5 C. J. Barbè, F. Arendse, P. Comte, M. Jirousek, F. Lenzmann, V. Shklover and M. Graetzel, *J. Am. Ceram. Soc.*, 1997, **80**, 3157.
6 K. Kato, A. Tsuzuki, H. Taoda, Y. Torii, T. Kato and Y. Butsugan, *J. Mater. Sci.*, 1994, **29**, 5911.
7 Y. Kotani, A. Matsuda, M. Tatsumisago, T. Minami, T. Umezawa and T. Kogure, *J. Sol-Gel Sci. Technol.*, 2000, **19**, 585.
8 L. Kavan, M. Graetzel, J. Rathousky and A. Zukal, *J. Electrochem. Soc.*, 1996, **143**, 394.
9 Y.-F. Chen, C.-Y. Lee, M.-Y. Yeng and H.-T. Chiu, *Mater. Chem. Phys.*, 2003, **81**, 39.
10 C.-C. Wang and J. Y. Ying, *Chem. Mater.*, 1999, **11**, 3113.
11 R. L. Penn and J. F. Banfield, *Geochim. Cosmochim. Acta*, 1999, **63**, 1549.
12 L. B. McCusker, R. B. Von Dreele, D. E. Cox, D. Louer and P. Scardi, *J. Appl. Crystallogr*, 1999, **32**, 36.
13 R. J. Hill and C. J. Howard, *J. Appl. Crystallogr.*, 1987, **20**, 467.
14 A. Altomare, M. C. Burla, C. Giacovazzo, A. Guagliardi, A. G. G. Moliterni, G. Polidori and R. Rizzi, *J. Appl. Crystallogr.*, 2001, **34**, 392.
15 S. Ardizzone and S. Trasatti, *Adv. Colloid Interface Sci.*, 1996, **64**, 173.
16 F. Bertoni, C. Galassi, S. Ardizzone and C. L. Bianchi, *J. Mater. Res.*, 2000, **15**, 164.
17 J. Beukenkamp and K. D. Herrington, *J. Am. Chem. Soc.*, 1960, **82**, 3025.
18 A. Liberti, V. Chiantella and F. Corigliano, *J. Inorg. Nucl. Chem.*, 1963, **25**, 415.
19 H. Zhang and J. F. Banfield, *Am. Mineral.*, 1999, **84**, 528.
20 R. L. Penn and J. F. Banfield, *Am. Mineral.*, 1999, **84**, 871.
21 A. A. Gribb and J. F. Banfield, *Am. Mineral.*, 1997, **82**, 717.
22 D. C. Hague and M. J. Mayo, *Nanostruct. Mater.*, 1993, **3**, 61.